Assessing the sensitivity of modeled air-sea CO_2 exchange to the remineralization depth of particulate organic and inorganic carbon

Birgit Schneider,[1,2] Laurent Bopp,[1] and Marion Gehlen[1]

Received 4 September 2007; revised 13 April 2008; accepted 12 May 2008; published 23 August 2008.

[1] To assess the sensitivity of surface ocean pCO_2 and air-sea CO_2 fluxes to changes in the remineralization depth of particulate organic and inorganic carbon (POC, PIC), a biogeochemical ocean circulation model (PISCES) was run with different parameterizations for vertical particle fluxes. On the basis of fluxes of POC and PIC, productivity, export, and the distributions of nitrogen (NO_3), dissolved inorganic carbon (DIC), and alkalinity, a number of indices defined to estimate the efficiency of carbon transport away from the atmosphere are applied. With differing success for the respective indices the results show that the more efficient the vertical transport of organic carbon toward depth, the lower the surface ocean pCO_2, the higher the air-sea CO_2 flux, and the stronger the increase in the oceanic inventory of DIC. Along with POC flux it is important to consider variations in PIC flux, as the net effect of particle flux reorganizations on surface ocean pCO_2 is a combination of changes in DIC and alkalinity. The results demonstrate that changes in the mechanistic formulation of vertical particle fluxes have direct and indirect effects on surface ocean pCO_2 and may thus interact with the atmospheric CO_2 reservoir.

Citation: Schneider, B., L. Bopp, and M. Gehlen (2008), Assessing the sensitivity of modeled air-sea CO_2 exchange to the remineralization depth of particulate organic and inorganic carbon, *Global Biogeochem. Cycles*, *22*, GB3021, doi:10.1029/2007GB003100.

1. Introduction

[2] Rising atmospheric CO_2 levels since the beginning of industrialization are largely responsible for a detectable warming of the Earth's atmosphere and oceans [*Solomon et al.*, 2007]. Together with solubility-driven CO_2 uptake by the surface water, substantial changes in the physical and chemical properties of the ocean take place. For example, temperature-driven changes in ocean circulation and increased stratification, as well as changes in the carbonate chemistry of sea water result in a reorganization of the vertical distributions of carbon and nutrients. As a consequence, marine ecosystems are predicted to be altered in their structure and functioning [*Sarmiento et al.*, 2004; *Boyd and Doney*, 2002; *Bopp et al.*, 2001]. This will eventually affect the efficiency of the ocean for uptake and storage of (anthropogenic) carbon from the atmosphere.

[3] The biological pump [*Volk and Hoffert*, 1985] transfers carbon bound into particulate organic carbon (POC) from the sunlit surface layer to the oceans interior where it becomes partly or entirely remineralized. The resulting loss of dissolved inorganic carbon (DIC) at the sea surface is either replaced by upwelling of DIC from below or by CO_2 gas exchange with the atmosphere. The timescale at which carbon is removed from air-sea exchange depends on its depth of remineralization, ranging from days for shallow remineralization in well-mixed waters to geological timescales for the fraction to be buried in marine sediments. The formation and flux of particulate inorganic carbon (PIC = $CaCO_3$), also called the calcium carbonate counter-pump, acts in terms of pCO_2 into the opposite direction. According to the reaction

$$Ca^{2+} + 2HCO_3^- \leftrightarrow CaCO_3 + CO_2 + H_2O \qquad (1)$$

when PIC precipitates, CO_2 is released. Consequently, high production and subsequent flux of PIC toward depth may increase surface ocean pCO_2 and potentially result in outgassing of CO_2 to the atmosphere. Vice versa, when PIC dissolves, CO_2 is consumed. In the surface ocean, reduced $CaCO_3$ precipitation increases the capacity of the ocean to absorb CO_2 from the atmosphere.

[4] The mechanisms that transform carbon from primary production into export flux and especially the resulting shape of particle flux curves toward greater depth are currently not very well understood [*Boyd and Trull*, 2007]. In ocean biogeochemical modeling, formulations of regionally variable particle flux parameterizations with prognostic particle settling velocities have been shown to be superior to those with constant sinking speeds or prescribed particle flux curves [*Kriest and Oschlies*, 2008; *Gehlen et al.*, 2006; *Howard et al.*, 2006]. Processes like mineral ballasting [*Klaas and Archer*, 2002; *Armstrong et*

[1]Laboratoire du Climat et de l'Environnement, Gif sur Yvette, France.
[2]Now at Institute of Geosciences, University of Kiel, Kiel, Germany.

0886-6236/08/2007GB003100

Table 1. Names, Short Description of Particle Flux Parameterization, and Reference to *Gehlen et al.* [2006] for the Model Experiments Analyzed in the Current Study

Experiment	Description	*Gehlen et al.* [2006]
REF	high flux feeding with aggregation	STD3
LFA	low flux feeding with aggregation	STD1
LFN	low flux feeding without aggregation	STD2
K&E	aggregation scheme [*Kriest and Evans*, 2000]	K&E
BAL	ballast parameterization	BAL

al., 2002; *Francois et al.*, 2002] and aggregate formation seem to be equally important, affecting density and size and thus sinking speeds of marine particles [*Passow and De La Rocha*, 2006]. Climate change is likely to affect marine biogeochemical cycles by changes in temperature, stratification, nutrient availability, and dust input, which results in alterations of marine productivity via changes in marine productivity and species compositions. This in turn will affect mineral ballasting of organic carbon fluxes toward depth in the water column and may thus impact the partitioning of carbon between atmosphere and ocean.

[5] To test the sensitivity of surface ocean pCO_2 and air-sea CO_2 gas exchange to changes in the vertical flux of POC and PIC in the water column, a biogeochemical ocean circulation model (OPA8.1/PISCES) was run with five parameterizations for particle fluxes, starting from the same initial conditions [*Gehlen et al.*, 2006]. The current study investigates the efficiency of the vertical flux of POC and PIC in the water column in terms of downward carbon transport away from the atmosphere. In particular, changes in surface ocean pCO_2, air-sea CO_2 flux, as well as productivity, DIC, alkalinity, and nutrient (NO_3) concentrations are analyzed. The results show that reorganizations in marine particle fluxes may have an immediate and persistent effect on atmospheric and oceanic carbon reservoirs.

2. Model and Experiments

[6] The model used for the current investigation is the OPA8.1/PISCES ocean circulation marine biogeochemical model. The physical forcing fields to run the PISCES model are provided by the OPA8.1 ocean circulation model that is driven by a constant climatological atmospheric forcing on the basis of NCEP/NCAR reanalysis data. The ocean and biogeochemical models are run on the ORCA2.0 grid with a horizontal resolution of $2^\circ \times 2$ cos latitude and 30 vertical levels with layer thickness increasing over depth from 10 m for the upper 10 levels to 500 m at depth. A detailed description of the ocean physical model can be found in the work of *Madec et al.* [1998].

[7] The PISCES marine ecosystem model [*Aumont and Bopp*, 2006] simulates the biogeochemical cycling of the major nutrients phosphate (PO_4), nitrate (NO_3), ammonium (NH_4), silicate ($SiOH_4$), and iron (Fe) next to dissolved inorganic carbon (DIC), oxygen (O_2), and total alkalinity (TALK). The model has two phytoplankton size classes (big and small), representing nanophytoplankton and diatoms and two zooplankton size classes (big and small) for microzooplankton and mesozooplankton. The pool of sinking POC is fueled by mortality and grazing of zooplankton. Semilabile dissolved organic carbon (DOC) is produced via excretion by all plankton types during grazing and the decay of POC. Loss terms of DOC are decay and aggregation onto POC. There is no calcite attached to living cells in the model, and sinking PIC material is produced by mortality of nanophytoplankton and zooplankton grazing on nanophytoplankton. Detrital opal is a result of diatom mortality and mesozooplankton grazing on diatoms.

[8] Five different parameterizations to describe the vertical flux of particles in the water column are applied in the current study (Table 1). An in-depth description of the different particle flux parameterizations used in the current study including the underlying equations and comparisons with observational data of particle fluxes, ocean sediments, satellite data, and dissolved tracer distributions is given by *Gehlen et al.* [2006]; here we will briefly sum up the major differences between the five parameterizations. In the initial simulation (REF), small particles are sinking with a constant sinking speed of 3 m/d, while for large particles (large POC, PIC, opal), sinking speeds are 50 m/d in the mixed layer, increasing over depth. In the model there is aggregation of DOC on small and large POC as well as from small POC to large POC, which increases the pool of large particles. A flux-feeding parameterization is implemented to account for the observation that certain mesozooplankton preferentially feed on fast sinking particles. This mechanism breaks up large POC into small particles, reducing the overall POC flux most notably between 100 and 1000 m. In general, particle flux attenuation is a result of temperature-dependent mineralization and zooplankton excretion transferring POC into semilabile DOC, which is decaying with a lifetime of several weeks to months. In the experiments LFA and LFN, particle fluxes are similarly parameterized, but flux-feeding intensities are lower. LFA also includes particle aggregation like in REF, whereas in LFN no aggregation takes place. In the experiment K&E, which realizes an aggregation parameterization based on *Kriest and Evans* [2000], there is no distinction between different particle size classes, but rather a continuous particle size spectrum is modeled. Sinking speeds are computed prognostically as a function of the respective particle size spectrum. In the ballast parameterization (BAL), where only POC, PIC, and opal are considered, sinking speeds are a function of the composition of the particle pool and assigned to be identical for all types of particles. For more details about the general characteristics of the PISCES model, see *Aumont and Bopp* [2006].

[9] The five different particle flux parameterizations are applied to the same initial state, on the basis of an equilibrium run (3000 years) of REF to estimate the response of surface ocean pCO_2 and air-sea CO_2 exchange to changes in the remineralization depth of POC in the water column. All simulations were integrated over 100 years under a constant climatological ocean circulation field that exhibits seasonal but no interannual variability and which remains constant for all experiments over the course of the simulations. Atmospheric pCO_2 is fixed to a preindustrial value of 278 ppm. Results for the different particle flux parameterizations are compared to REF, which was also integrated over another

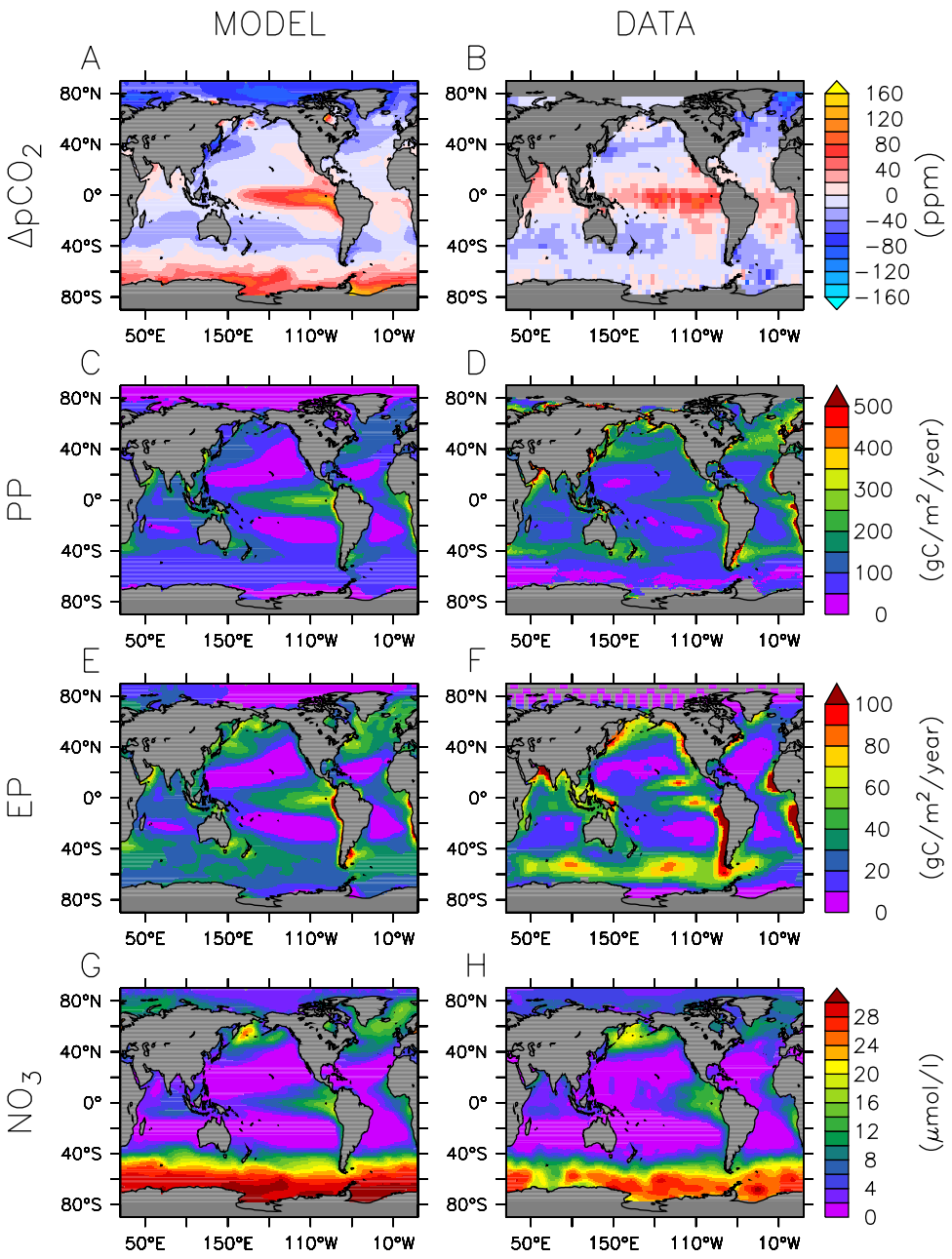

Figure 1. (a) Modeled global annual fields of preindustrial ΔpCO_2 and (b) ΔpCO_2 recent climatology from *Takahashi et al.* [2002]. (c) Modeled fields of global annual primary production (PP) and (d) ocean color derived PP estimates from *Behrenfeld et al.* [2006]. (e) Export production fields as obtained by the model and (f) results from inverse modeling [*Schlitzer*, 2000]. (g) Average of the surface 0–100 m NO_3 concentrations from the model and (h) the climatology of the World Ocean Atlas (WOA) [*Conkright et al.*, 2002].

100 years, to exclude changes due to possible drift in the biogeochemical model. The integration time of 100 years is long enough to allow particle fluxes to adapt largely to the changes; however, it is much too short to yield new equilibria. Nevertheless, as conditions are the same for all simulations, a comparison of the results obtained is internally consistent and applicable for a sensitivity study. The long-term behavior of the observed trends is investigated by extending simulation BAL over 900 years, the results of which will also be presented.

3. Results

3.1. Reference State

[10] The reference state (REF) for all model experiments, which is representing preindustrial conditions, is in reason-

Table 2. Comparison of ΔpCO_2, Primary Production, POC Export, and Surface Water NO_3 Concentrations From the Modeled Reference State With Data and Observation-Based Estimates[a]

Variable	Model	Observation	Bias	R^2	rstd	Reference
ΔpCO_2 (ppm)	−3.91	−2.23	−1.68	0.14	1.06	*Takahashi et al.* [2002]
PP (GtC/a)	41.3	48.0	−6.7	0.23	0.51	*Behrenfeld et al.* [2006]
EP (GtC/a)	10.7	11.4	−0.7	0.26	0.63	*Schlitzer* [2000]
NO_3 (μmol/l)	6.97	6.58	0.39	0.88	1.20	*Conkright et al.* [2002]

[a]Shown are global annual average (ΔpCO_2, NO_3) or integrated (primary production (PP), POC export (EP)) values of the respective variables and the resulting bias (difference model observation), as well as spatial correlations (R^2) of annual average values and their ratios of standard deviations (rstd = std_{model}/std_{obs}).

able agreement with data and observation-based estimates for ΔpCO_2, primary production (PP), export production (EP) and surface water NO_3 concentrations (Figure 1). The large-scale pattern of surface ocean ΔpCO_2 distributions (pCO_2 difference sea-air) is well represented by the model, however, one has to keep in mind that preindustrial model fields are compared to modern observations that are affected by anthropogenic CO_2. Generally, high ΔpCO_2 values, which indicate outgassing of CO_2 from the ocean into the atmosphere, are located in the equatorial Pacific. In the Southern Ocean the model probably overestimates surface pCO_2. However, data are sparse from this remote ocean area and the role of the Southern Ocean as a natural source of CO_2 and its present behavior as a sink for anthropogenic CO_2 is currently heavily debated [*Le Quéré et al.*, 2007; *Mikaloff Fletcher et al.*, 2007]. The resulting global annual mean air-sea CO_2 flux in the model is −0.33 GtC/a, based on calculations with the gas exchange coefficient according to *Wanninkhof* [1992]. This means there is slight outgassing of CO_2, balancing carbon input from river discharge. The spatial correlation between modeled and climatological ΔpCO_2 fields is rather weak ($R^2 = 0.14$), but slightly better when taking into account the seasonal cycle ($R^2 = 0.29$). Global annual average values and standard deviations of modeled and observed ΔpCO_2 are in better agreement (Table 2).

[11] Vertically integrated PP amounts to 41.3 GtC/a globally, which is in the range of independent estimates derived from ocean color measurements [*Carr et al.*, 2006]. Compared to the PP compilation of *Behrenfeld et al.* [2006] spatial correlations are moderate (Table 2). Export production in the model is defined as the flux of particulate organic carbon (POC) across the 100 m depth level, adding up to 10.7 GtC/a. This is slightly lower than 11.4 GtC/a obtained from inverse modeling [*Schlitzer*, 2000]. The spatial agreement between both ($R^2 = 0.26$) is similar to the value obtained for PP (Table 2). Modeled surface water NO_3 concentrations match climatological values very well [*Aumont and Bopp*, 2006]. When averaged over the top 0–100 m of the water column, the bias is about 6% and spatial correlations are on the order of $R^2 = 0.88$ (Table 2). Modeled particle fluxes and the resulting sediment compositions have been extensively discussed and compared to observational data by *Gehlen et al.* [2006].

[12] In summary, the initial conditions of marine biogeochemical tracer distributions in the PISCES model are in reasonable agreement with independent estimates.

3.2. Reorganization of Marine Biogeochemical Cycles

[13] After 100 years of model integration applying five different particle flux parameterizations biogeochemical cycles have undergone considerable reorganization. The resulting global annual mean values of primary production, POC export across 100 m depth, ΔpCO_2, air-sea CO_2 flux and the total DIC inventory are displayed in Table 3. Please note that in the present sensitivity study effects may be unrealistic. Therefore, results should be regarded in terms of interactions and mechanisms rather than realism.

3.2.1. Particle Fluxes

[14] The instantaneous change of particle flux parameterizations causes adaptations in the vertical flux of all types of sinking particles, partly induced directly by changes in the mechanistic formulation of particle sinking, and more indirectly, by the ecosystem response to reorganizations of dissolved properties like nutrients, carbon and alkalinity. In the following we will try to separate such effects as far as possible by comparing the mechanistically expected particle flux responses with those obtained from the simulations.

[15] In experiment LFA, that uses low flux-feeding intensity compared to the reference situation, the overall flux of POC is expected to be increased, because fewer large particles are broken up into small ones increasing the mean POC sinking speed, while there should be no direct effect on PIC and opal fluxes. The simulation, however, shows a considerable decrease in the POC flux from the surface down to 300 m depth and higher than reference POC fluxes below (Figure 2a). PIC fluxes are strongly reduced everywhere in the water column while opal fluxes remain almost

Table 3. Global Annual Mean Values for Primary Production, POC Export, ΔpCO_2, CO_2-Flux, and DIC Inventory for All Experiments After 100 Years of Model Integration

Experiment	PP (GtC/a)	EP (GtC/a)	ΔpCO_2 (ppm)	CO_2Flux (GtC/a)	DIC Inventory (GtC)
REF	40.5	10.1	−5.2	−0.33	35765
LFA	25.9	8.0	−4.2	0.00	35796
LFN	28.2	7.6	−4.3	−0.07	35785
K&E	36.7	5.3	−1.6	−0.46	35746
BAL	21.0	11.2	−8.6	0.83	35915

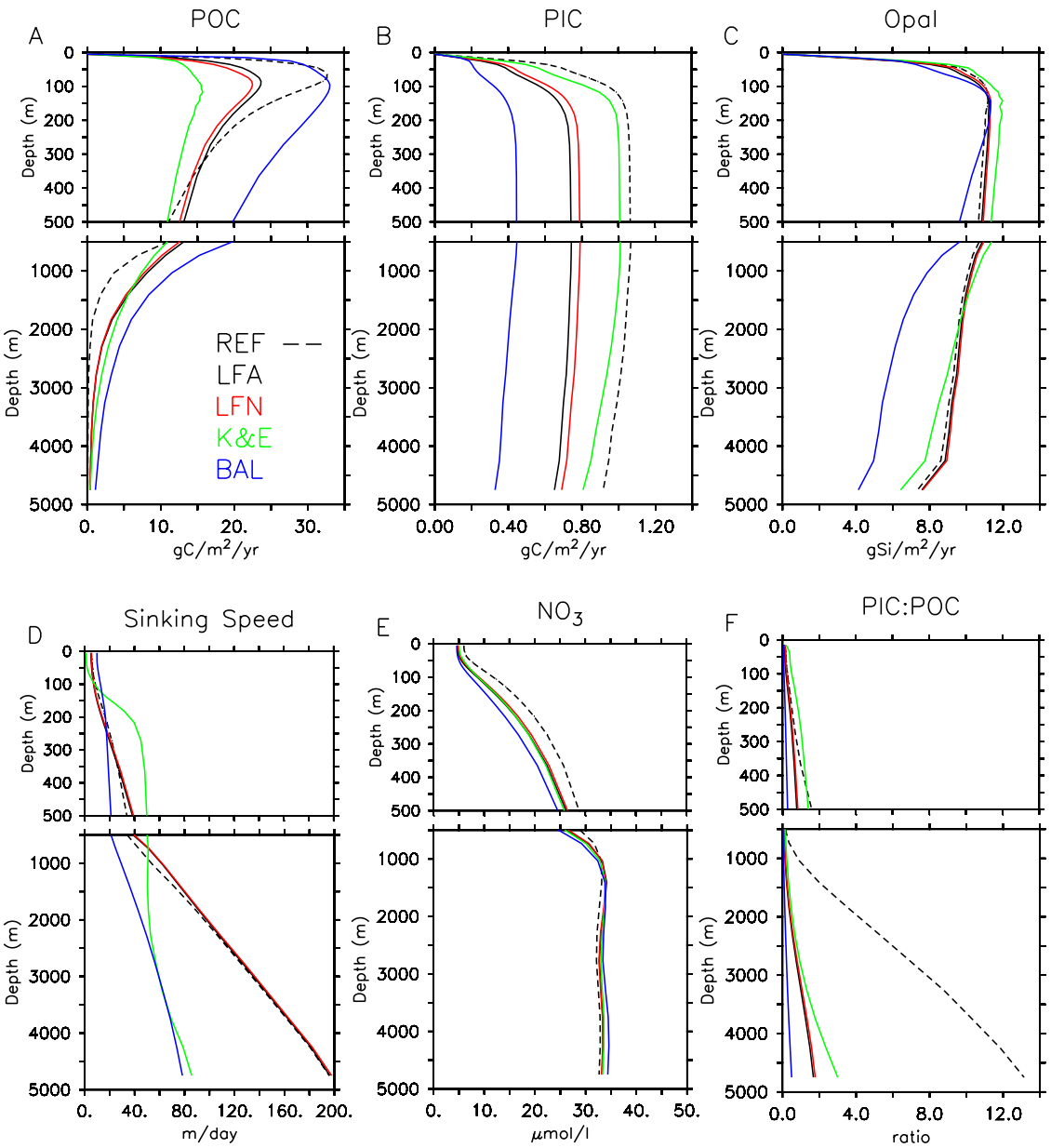

Figure 2. Profiles of vertical particle fluxes in the water column in the different model simulations for (a) POC, (b) PIC, (c) opal, (d) sinking speeds, (e) NO_3, and (f) the ratio of sinking $CaCO_3$ (PIC) to sinking POC. Please note the different scales for different types of particles (Figure 2a–2c) and a factor of 10 difference between the upper and lower panel of Figure 2f.

unchanged (Figures 2b and 2c). The lowering of POC and PIC fluxes can be explained by a reduction in surface water nutrient concentrations (Figure 2e) that reduce nanophytoplankton production and thus calcification, whereas diatom production only slightly decreases (Figure S1).[1] The effect of the lower flux-feeding intensity can be detected by the slightly higher sinking speeds than in REF below 300 m depth (Figure 2d) and elevated POC fluxes below this depth. Together, the reduced nanophytoplankton production and lower flux-feeding result in a considerable lowering of the ratio of PIC:POC transported toward depth (Figure 2f).

[16] Similar to LFA the parameterization LFN is expected to have no effect on the flux of PIC and opal, but for POC the impact of the low flux-feeding intensity favoring larger particles should be offset by reduced aggregate formation. The net effect on the POC flux compared to REF should be either an increased flux, but still lower than in LFA or even a net lowering when the absence of aggregation outcompetes the flux-feeding effect. However, very similar results as for LFA are found for all types of sinking particles (Figures 2a–2c), indicating that the standard aggregation

[1]Auxiliary materials are available in the HTML. doi:10.1029/2007GB003100.

scheme in the model has only a minor influence on particle fluxes. A weaker lowering of nanophytoplankton production compared to LFA (Figure S1) can explain the slightly higher PIC flux, whereas the slightly lower shallow (0–300 m) POC fluxes are due to the effect of absent aggregation.

[17] In K&E all particles sink with the same speed that is a function of the particle size spectrum. Having the same total mass, a spectrum consisting of less but larger particles will sink on average faster than a spectrum with more numerous but smaller particles. The type of particle (POC, PIC, opal) is therefore less important for the overall sinking speed than aggregate formation induced by turbulence as well as zooplankton feeding breaking up large particles into small ones. Because of the influence of water column and food web dynamics it is thus impossible to make a general conclusion on the expected sinking behavior of individual types of particles. The model results show a strong decrease in POC flux compared to REF above 500 m and a relative increase below (Figures 2a–2c). PIC flux is slightly reduced over the entire water column and opal flux is slightly enhanced between 50–2000 m depth and slightly reduced below. The strong reduction of shallow POC fluxes for K&E can only in part be explained by a reduction of primary production, as nanophytoplankton production is reduced while diatom production is slightly enhanced, particularly in the eastern equatorial Pacific (Figures S1–S3). From the sinking speed (Figure 2d) it comes out that overall sinking velocities are very low between the surface and 50 m depth and then increase strongly until 200 m depth below which they stay almost constant. Most probably, the very low sinking speeds near the surface increase the particle residence time and thus remineralization. From this enhanced nutrient turnover diatoms in the equatorial east Pacific benefit the most, responding with slightly higher opal fluxes [*Gehlen et al.*, 2006]. The faster turnover of carbon and nutrients at the surface is also shown by only a minor reduction of nanophytoplankton growth, although total NO_3 concentrations are reduced (Figures S4 and S1).

[18] In the parameterization BAL, where all particles are sinking with the same speed dependent on the excess density (compared to seawater) of the entire particle pool, the expected net effect on the POC flux is also difficult to estimate. On the one hand, small particles that were sinking with low rates before will be accelerated because of ballasting by PIC and opal particles, on the other hand, large POC that were sinking at high rates before slow down the entire particle pool because of their low density. The contribution of both types of POC to the change in overall sinking speeds will therefore be dependent on their relative contributions. For the fluxes of PIC and opal lower sinking rates than before are expected as these two ballast fractions will by slowed down by the presence of low-density POC. The model results show no major changes for the POC flux above 100 m depth in BAL and strongly enhanced fluxes below (Figure 2a). PIC flux is strongly reduced everywhere up to −60% and opal fluxes are also reduced below 250 m depth. The high POC fluxes are in strong contrast to the change in primary production, where the BAL experiment undergoes the largest reductions for both nanophytoplankton and diatoms (Figures S1–S3) and also strongest nutrient depletion (Figure S5). While reductions in PIC and opal fluxes are in line with reduced productivity the high POC fluxes can only be explained by the contribution of small POC that are assigned sinking rates that are much higher than in REF, particularly above 200 m depth (Figure 2d). Below this depth the low density of large POC is responsible for a reduction of the overall sinking speeds.

[19] It is interesting to see that for all different particle flux parameterizations compared to REF a reduction in the vertical gradient of POC fluxes over depth occurs (Figure 2a) paralleled by a decrease in the vertical DIC distribution (not shown). This is a strong indication for more efficient downward POC transport in all simulations, which goes along with large-scale upper ocean (0–1000 m) nutrient depletion (Figures 2e and S5) and reduced primary production, except for diatom production in the equatorial east Pacific in K&E. Qualitatively, reduced nanophytoplankton production and thus calcification is consistent with reduced PIC fluxes and increased alkalinity concentrations for all simulations (Figure S4). In combination with higher POC fluxes at greater depth this results in extremely low PIC:POC ratios that are transported toward depth in all simulations compared to REF, suggesting a strong weakening of the calcium carbonate counter pump. In all simulations (including REF) the attenuation of PIC flux over depth in the water column is rather weak, indicating that there is too little pelagic $CaCO_3$ dissolution, a problem which has been overcome in a more recent version of the PISCES model [*Gehlen et al.*, 2007].

3.2.2. Surface Ocean Properties

[20] The rearrangement of particle fluxes in the water column as explained above results in alterations of surface ocean properties in all simulations. Interestingly, for all simulations in the eastern equatorial Pacific, the major outgassing region of the world ocean, pCO_2 (and surface water DIC) are strongly lowered, although on average global surface water pCO_2 does not change considerably for LFA and LFN (+1 ppm), while in K&E it is about 3.6 ppm higher and in BAL 3.4 ppm lower than in REF (Figures 3, S6, and Table 3). In all simulations the pCO_2 reduction in the eastern equatorial Pacific can be explained partly by the more efficient downward POC flux, however, in LFA, LFN and BAL a strong reduction of surface water DIC goes along with an increase in alkalinity from reduced calcification (Figure S6), which further reduces pCO_2. In K&E a similarly strong reduction in DIC is followed only by a minor increase in alkalinity because of a small reduction in calcification, here. This lower decrease in pCO_2 is mirrored in the lowest reduction of CO_2 outgassing in this area for K&E (Figure S7). In BAL that experiences the strongest reduction of calcification, globally and in the eastern equatorial Pacific, the reduction of pCO_2 in the latter region is strongest among the simulations tested here and also the outgassing from this region is most strongly reduced. Together with elsewhere increasing pCO_2 this results for K&E in globally higher surface water pCO_2 and more net outgassing than in REF, while globally lower pCO_2 in BAL yields a switch to net CO_2 uptake. Both global net changes of pCO_2 and CO_2 flux are minor for LFA and LFN, that end up being more or less neutral in terms of CO_2 exchange. In general, the spatial distribution of the

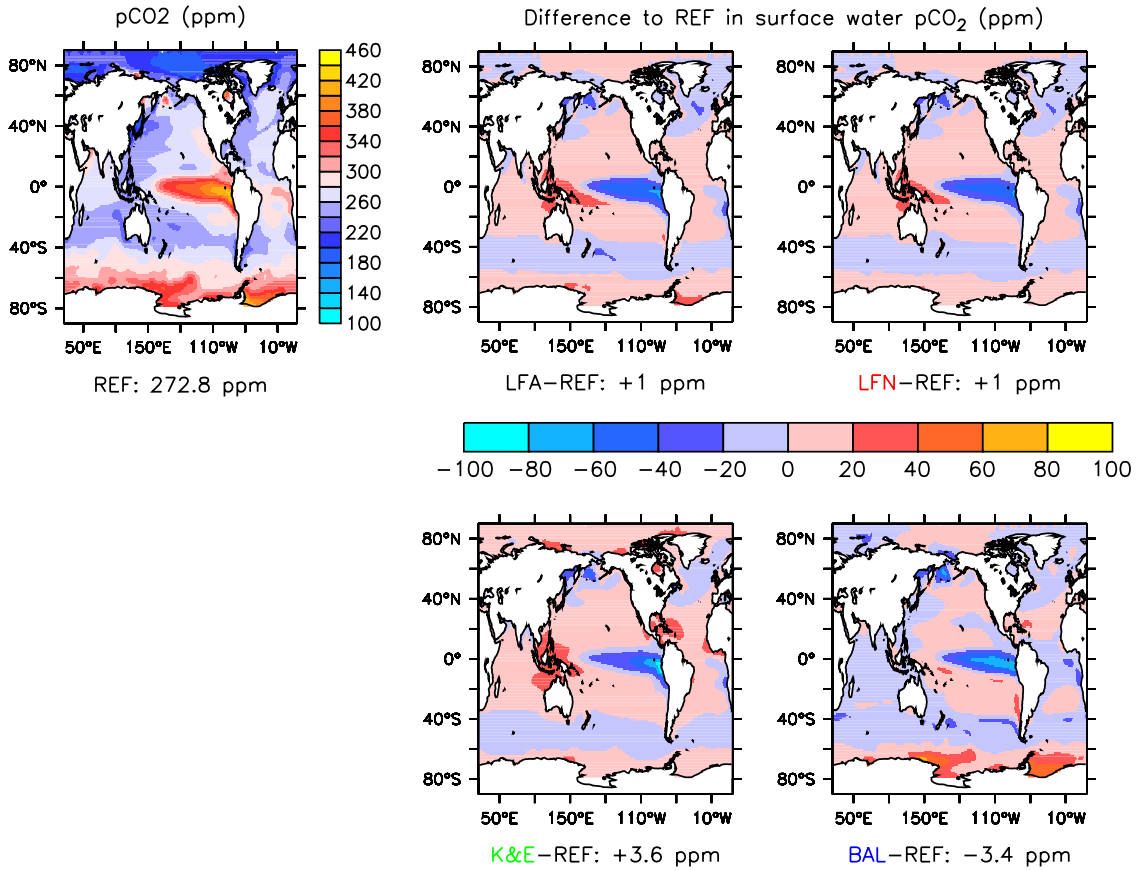

Figure 3. (top left) Surface ocean pCO_2 in the reference simulation (REF). (other panels) Changes in surface ocean pCO_2 of the respective particle flux parameterization relative to REF. For the differences, positive (negative) values indicate either less (more) CO_2 uptake or more (less) CO_2 outgassing by the ocean.

changes in air-sea CO_2 exchange is the inverse of the changes in surface pCO_2 (Figure S7). There are strong anticorrelations with high correlation coefficients between the changes in pCO_2 and air-sea CO_2 exchange for LFA and LFN ($R^2 = 0.83$) as well as for K&E ($R^2 = 0.81$) and BAL ($R^2 = 0.75$).

4. Assessing Particle Flux Efficiency

[21] The amount of POC export cannot be measured directly on larger spatial and temporal scales, nor the efficiency of its transport toward depth. Therefore, many efforts were undertaken to estimate both, for example from sediment trap deployments, dissolved nutrient concentrations, geochemical tracer studies or ocean color measurements from space. An extensive review of what is currently known about the export of biogenic particles in the ocean is given by *Boyd and Trull* [2007]. Here, only a brief description of the measures to estimate carbon flux efficiency that are applied in the current study is given. Changes in particle flux efficiency from the different experiments are then related to changes in (surface) ocean properties like nutrient concentrations, productivity, pCO_2, air-sea CO_2 exchange and the DIC inventory. Especially the latter is important, because it shows the cumulative effect over the 100 year integration, whereas pCO_2 and air-sea CO_2 exchange are still subject to the transient behavior of the system moving toward a new equilibrium. With this analysis assets and drawbacks of the individual approaches as well as their applicability as a measure for the source/sink behavior of the surface ocean for atmospheric CO_2 can be identified and assessed.

[22] A conceptually simple and straightforward approach to assess particle flux efficiency is to relate particle fluxes from the same station at different depths. This was done in terms of "transfer efficiency" (TE) in a study by *Buesseler et al.* [2007], who relate particle fluxes from sediment traps at 500 m depth to 150 m depth and in another study by *Francois et al.* [2002], covering a larger depth range by relating fluxes between 2000 m and surface export as derived from satellite measurements of ocean color [*Laws et al.*, 2000]. Sediment trap data, however, suffer from problems of trapping efficiency [*Usbeck et al.*, 2003] induced by turbulence in the water column and by dissolution of material in the cups of the sampling device [*Kähler and Bauerfeind*, 2001]. The first can partly be overcome by application of neutrally buoyant sediment traps [*Buesseler et al.*, 2007] and design of particle interceptors [*Gust et al.*, 1994], the latter by poisoning of the liquid in the sampling cups. The result of TE is dimensionless, so that an overall low flux that has little attenuation over depth suggests a high TE. This makes TE rather a measure of biological

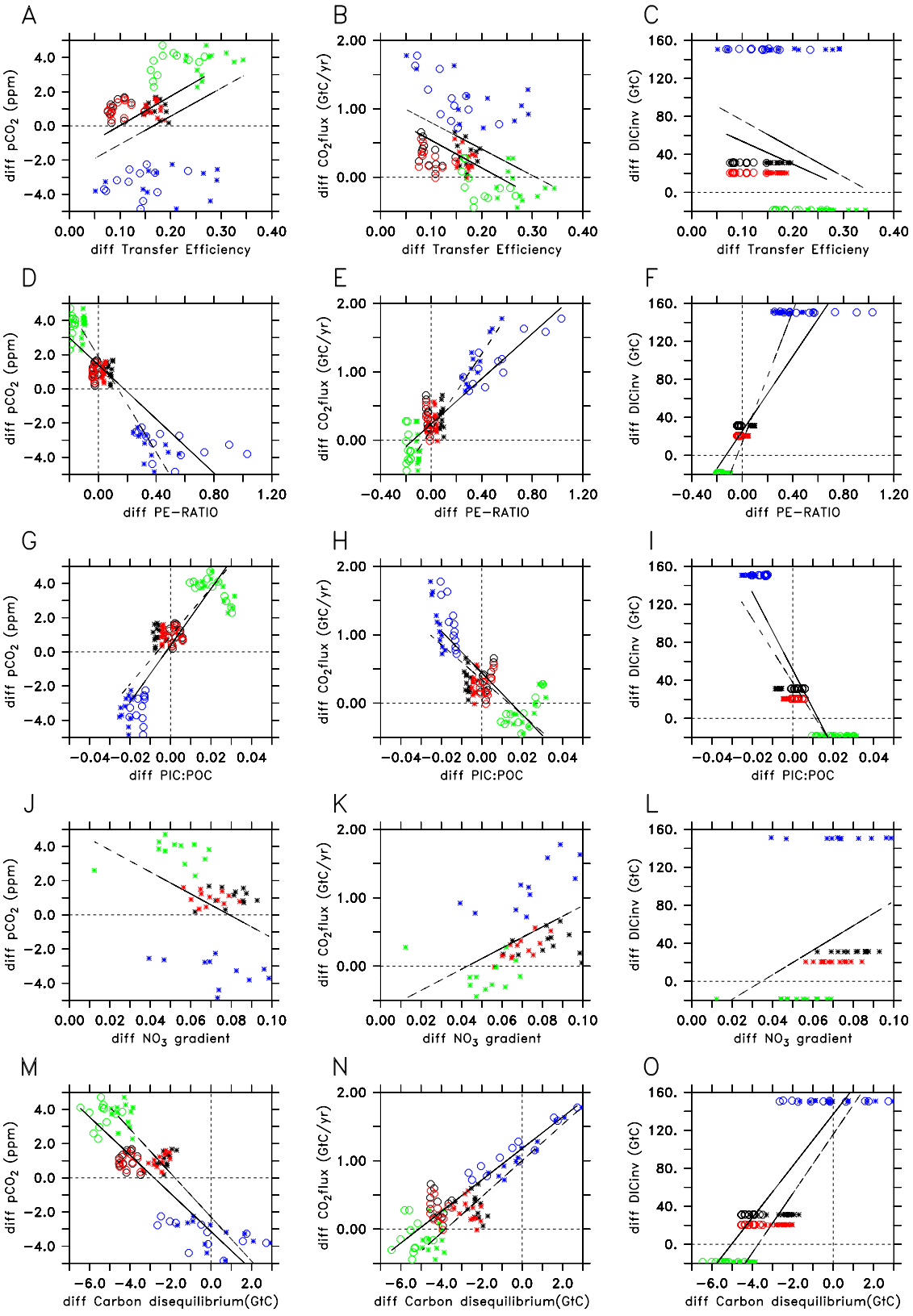
A
B
C
D
E
F
G
H
I
J
K
L
M
N
O
diff pCO2 (ppm)
diff CO2flux (GtC/yr)
diff DICinv (GtC)
diff Transfer Efficiency
diff Transfer Efficieny
diff PE−RATIO
diff PIC:POC
diff NO3 gradient
diff Carbon disequilibrium(GtC)

Figure 4

Table 4. Correlation Coefficients and Slopes of the Regression Lines of Estimates for Particle Flux Efficiency Versus Surface Ocean pCO_2, Air-Sea CO_2 Flux, and DIC Inventory[a]

	pCO_2		CO_2Flux		DIC Inventory	
	R^2	Slope	R^2	Slope	R^2	Slope
TE_{BUE}	0.15	16.43	0.21	−3.87	0.08	−296
TE_{FRA}	0.12	17.13	0.16	−4.04	0.04	−240
PE_{100}	0.90	−13.97	0.87	2.78	0.91	345
PE_{MLD}	0.80	−7.90	0.85	1.65	0.82	197
$PIC:POC_{100}$	0.77	140.20	0.63	−26.63	0.73	−3361
$PIC:POC_{MLD}$	0.74	166.90	0.61	−30.49	0.74	−4085
$NO_3\text{-}GRAD_{100}$	0.18	−64.15	0.24	15.49	0.12	1293
$C\text{-}DISEQ_{100}$	0.81	−1.29	0.84	0.26	0.79	31.2
$C\text{-}DISEQ_{MLD}$	0.81	−1.15	0.84	0.23	0.80	27.3

[a]For the calculations of the different measures for particle flux efficiency, please see text and caption of Figure 4.

turnover efficiency. In terms of oceanic CO_2 uptake capacity, it is of limited value locally, but a reasonable estimate on a basinwide or global scale.

[23] Applied to our model results, two TE estimates are computed as the ratio of POC flux in 500 m to 150 m

$$TE_{BUE} = \frac{POC_{flux,500}}{POC_{flux,150}} \tag{2}$$

and the ratio of POC flux in 2000 m to 100 m

$$TE_{FRA} = \frac{POC_{flux,2000}}{POC_{flux,100}}. \tag{3}$$

[24] For each experiment the difference to experiment REF of the global monthly mean TE value is computed and related to the respective difference in surface ocean pCO_2, air-sea CO_2 flux and global DIC inventory. All simulations experience a more or less well pronounced increase in TE compared to REF, however, correlations with the resulting changes in pCO_2, air-sea CO_2 flux and DIC are very low (Figures 4a–4c and Table 4).

[25] Another approach to assess carbon export efficiency is the relation of carbon export to productivity, called the PE ratio [*Dunne et al.*, 2005; *Laws et al.*, 2000]. It is a matter of definition which depth level the amount of carbon export refers to. For reasons of simplicity, especially in model frameworks often the 100 m depth level is chosen. Otherwise, the depth of the euphotic zone (1% light level) or the mixed layer depth are taken as lower boundaries. A modeling study by *Oschlies and Kähler* [2004] has shown that with respect to uptake and storage of CO_2 from the atmosphere the depth of the maximum (winter) mixed layer (MLD_{max}) is of major importance. For the PE ratio, like for TE, the argument of being dimensionless and thus rather a good measure on a basinwide or global scale, exists.

[26] In our study, PE ratios are computed as global monthly integrals, once over the 100 m depth level (PE_{100}) and once over MLD_{max}(PE_{MLD}). Therefore the ratio of POC flux across the respective depth layer over the amount of primary production within the respective zone is taken as

$$PE_{100} = \frac{POC_{flux,100}}{PP_{0-100}} \tag{4}$$

and

$$PE_{MLD} = \frac{POC_{flux,MLD\mathrm{MAX}}}{PP_{0-MLD\mathrm{MAX}}}. \tag{5}$$

[27] This computation neglects export of DOC via subduction, which may make up 40% of total export, as shown by intercomparison of OCMIP-2 model results [*Najjar et al.*, 2007]. Nevertheless, the changes in both PE ratios induced by the different particle flux parameterizations show very high correlations with the changes in surface ocean pCO_2, air-sea CO_2 flux and DIC with correlation coefficients on the order of $R^2 = 0.80–0.91$ (Figures 4d–4f and Table 4). In LFA and LFN, PE ratios stay rather constant, whereas in K&E they decrease and in BAL they increase. As expected, a reduced (increased) PE ratio results in higher (lower) surface ocean pCO_2, negative (positive) air-sea CO_2 flux and finally in lower (higher) DIC inventory. It is interesting to see, that although MLD_{max} should be the more important reference level, PE ratios over 100 m show slightly higher correlations.

[28] As next to POC also the flux of PIC determines the efficiency of downward carbon transport, either as ballast material [*Klaas and Archer*, 2002; *Armstrong et al.*, 2002] or with regard to the efficiency of the carbonate counter pump, PIC:POC ratios of sinking particles can also be taken

Figure 4. Regressions of different estimates of particle flux efficiency versus surface ocean pCO_2 (left column), air-sea CO_2 flux (middle column), and total DIC inventory (right column). Displayed are the differences to REF of global monthly mean values of the individual simulations ((black) LFA; (red) LFN; (green) K&E, (blue) BAL). Particle flux efficiency is computed as (a–c) the transfer efficiency (TE) according to *Buesseler et al.* [2007] as the ratio of POC flux at 500 m to 150 m (stars, dashed regression line) and according to *Francois et al.* [2002] (circles, full regression lines) as the ratio of POC flux in 2000 m to export flux (here: POC flux at 100 m); (d–f) the PE ratio, which is the ratio of POC export over primary production, once calculated at 100 m depth (stars, dashed regression line) and once over MLD_{MAX} (circles, full regression line); (g–i) the ratio in the export of PIC over POC across 100 m (stars, dashed regression line) and MLD_{MAX} (circles, full regression line; (j–l) the vertical gradient in NO_3 concentrations [*Sarmiento and Gruber*, 2006]; (M–O) the carbon disequilibrium (C-DISEQ), which is the difference between the amount of carbon that is transported downward by particle flux (POC, PIC) and the carbon that is upwelled as DIC and alkalinity, also computed once over 100 m depth (stars, dashed regression line) and once over MLD_{MAX} (circles, full regression line). The corresponding correlation coefficients and slopes of the regression lines are given in Table 4. More details about calculation of the different estimates are given in the text.

as a flux efficiency measure. This approach also does not take into account DOC export, but alkalinity effects.

[29] As done before for the PE ratios, modeled changes in the PIC:POC flux ratios are computed as global monthly averages, once at 100 m depth and once at MLD_{max} as

$$PIC : POC_{100} = \left(\frac{PIC}{POC}\right)_{flux,100} \quad (6)$$

and

$$PIC : POC_{MLD} = \left(\frac{PIC}{POC}\right)_{flux,MLD\mathrm{MAX}}. \quad (7)$$

[30] The resulting correlations between changes in the PIC:POC ratios and pCO_2, air-sea CO_2 flux and DIC are moderate and on the order of $R^2 = 0.61–0.77$ (Figures 4g–4i and Table 4). Similar to the PE ratio, in LFA and LFN the changes in PIC:POC ratios are low. In K&E, where there is a lowering of PE ratios the PIC:POC ratios increase, in BAL vice versa. An increase (decrease) in the PIC:POC ratio is accompanied by higher (lower) pCO_2, lower (higher) air-sea CO_2 exchange and a lower (higher) DIC inventory. For all experiments there are only minor differences between the PIC:POC ratios at 100 m and MLD_{max}.

[31] Experiment BAL is the only parameterization that explicitly takes into account the mineral fraction to determine the overall settling velocity of sinking particles. It experiences the strongest reductions in nanophytoplankton and diatom production (Figures S1–S3) and thus calcification and opal production. Consequently, one might expect a reduction in the efficiency of the vertical POC transport due to less ballasting material. Especially PIC is important in the real ocean, where it has been demonstrated to be the most important carrier of POC toward depth [*Klaas and Archer*, 2002; *Francois et al.*, 2002]. On the other hand, as all particles sink with the same speed in BAL, the ballast fractions PIC and opal considerably increase the flux of small POC, which results in relatively high total POC fluxes toward depth (Figure 2a). This result shows that changes in the ballasting of POC fluxes may have a particularly strong influence on surface ocean pCO_2 and thus the atmospheric and oceanic carbon reservoirs.

[32] A more indirect approach to assess carbon export efficiency is the use of vertical gradients in NO_3 concentrations, applied by *Sarmiento and Gruber* [2006] as the "biological pump efficiency". Assuming that without any biogeochemical cycling NO_3 in the ocean would be homogeneously distributed, its vertical gradient can be taken as a measure for efficiency of the biological pump, which means both particulate and dissolved organic carbon export. This approach, however, does not take into account effects of the carbonate counter pump (neither do TE and the PE ratio, which were explained above), preferential remineralization of particulate organic nitrogen compared to POC, which was derived from sediment trap data [*Schneider et al.*, 2003] or nitrogen fixation and denitrification, which would both lower the vertical NO_3 gradient. Nevertheless, it is an approach that tries to balance downward fluxes of particulate and dissolved organic material with upward transport and mixing of inorganic nutrients.

[33] Applied to our model results, the global monthly mean gradients of NO_3 concentrations are computed like in the work of *Sarmiento and Gruber* [2006] as the gradients between the two depth layers 0–100 m (surface) and 100–200 m (deep):

$$NO_3 - GRAD = \frac{NO_{3,100-200} - NO_{3,0-100}}{NO_{3,100-200}}. \quad (8)$$

[34] The higher the value of NO_3-GRAD, the more efficient the biological pump. Compared to REF all simulations show only minor changes in NO_3-GRAD (Figures 4j–4l). Correlations with the concomitant changes in pCO_2, air-sea CO_2 flux and global DIC inventory are low, between $R^2 = 0.12$ and 0.24 (Table 4). As only the top 200 m of the water column are considered, shallow carbon remineralization between 100 and 200 m might suggest a high carbon export efficiency, while remineralization below 200 m results in low gradients, suggesting a low efficiency. On the other hand, the application of this method will be influenced by the fact that the dissolved tracer distributions are not in equilibrium.

[35] Actually, it is the balance between downward (particle flux, subduction) and upward (upwelling and mixing) transport of DIC and alkalinity that finally determines the net effect of changes in organic and inorganic carbon export on surface ocean pCO_2 and thus CO_2 gas exchange. To account for this balance, we compute another efficiency estimate that relates the downward carbon flux as the difference between POC and PIC flux (because both act into different directions on surface pCO_2) to the difference in advective upward (downward) transport of DIC (DOC) and alkalinity. The measure C-DISEQ is computed once over the 100 m depth level and once over MLD_{max}:

$$C - DISEQ_{100} = (POC - PIC)_{flux,100} - (DIC + DOC - TALK)_{upw,100} \quad (9)$$

and

$$C - DISEQ_{MLD} = (POC - PIC)_{flux,MLD\mathrm{MAX}} - (DIC + DOC - TALK)_{upw,MLD\mathrm{MAX}}. \quad (10)$$

[36] To take into account the nonlinearity of the carbonate system such that a change in PIC (and alkalinity) has a lower absolute effect on the pCO_2 than the same amount of POC (DOC, DIC) change the fluxes of PIC and alkalinity are multplied by a nonlinearity factor. The latter is computed for each model grid point as the ratio of the pCO_2 change induced by 1 μmol/l PIC dissolution over 1 μmol/l POC dissolution. For the PIC dissolution a DIC increase of 1 μmol/l and an alkalinity increase of 2 μmol/l is taken and divided by 1 μmol/l DIC increase because of POC mineralization. As both act into different directions the absolute value of this ratio is used for multiplication with the PIC and alkalinity fluxes. The derived nonlinearity factor shows a

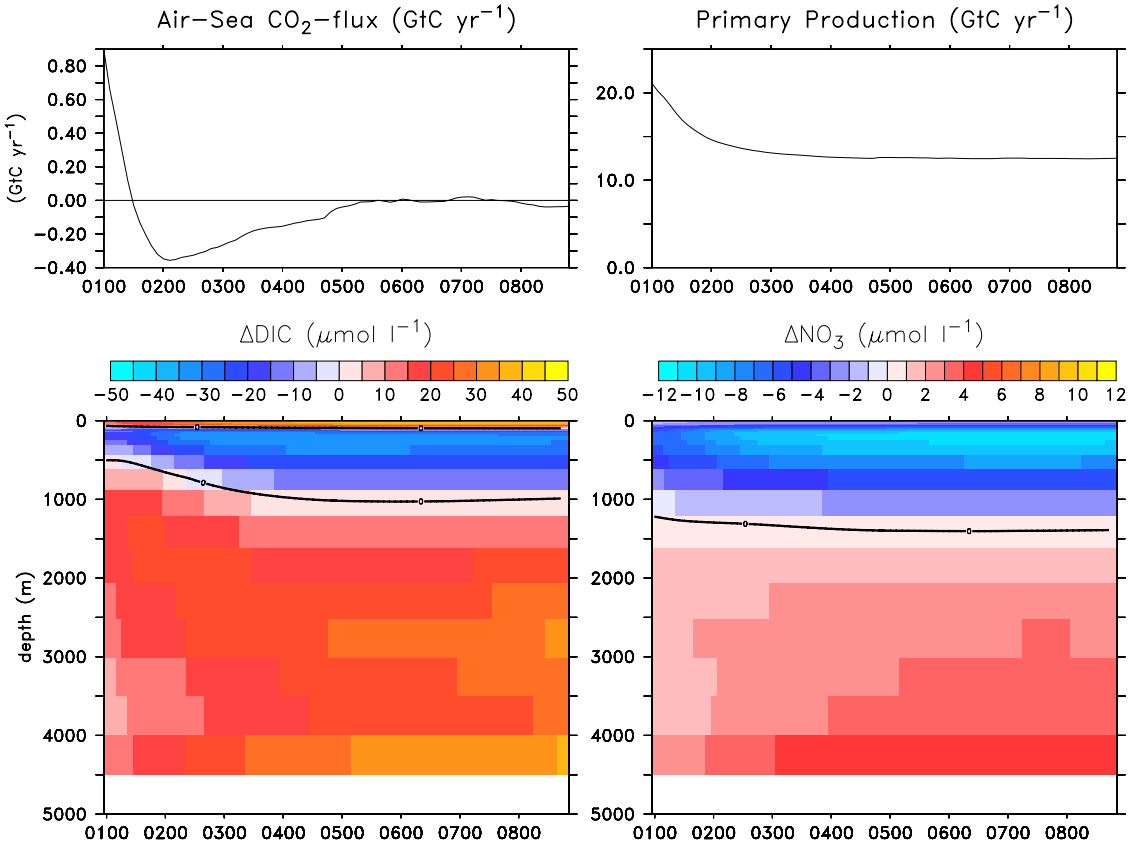

Figure 5. Time series of (top left) air-sea CO_2-flux and (top right) primary production (PP) for the BAL simulation, as well as Hovmöller diagrams showing the vertical distribution of changes in (bottom left) DIC and (bottom right) NO_3 in BAL relative to REF.

strong latitudinal dependence with values around 0.9 at high latitudes and values around 0.45 in the tropics.

[37] Upwelling of DIC and alkalinity is computed on each model grid point from the respective concentrations multiplied with the local vertical velocities (alkalinity also with the nonlinearity factor) and then integrated over the global ocean domain. The resulting efficiency estimate C-DISEQ has the advantage of having the same dimension as carbon fluxes. When it is positive more organic carbon is transported downward than inorganic carbon is upwelled. Ideally, when matching the exact depth layer and the surface ocean has enough time to equilibrate the air-sea pCO_2 difference C-DISEQ should be zero in steady state when upward and downward transports are balanced or it should equal the air-sea gas exchange.

[38] However, some drawbacks in the calculation of C-DISEQ still exist. First, the upwelling of DIC and TALK is computed by using concentrations and vertical velocities, so that diffusive mixing is not taken into account and, second, the (minor) effect of POC flux on alkalinity due to changes in NO_3 concentrations is neglected here. The results, however, are convincing with high correlation coefficients ($R^2 = 0.79–0.84$) between changes in C-DISEQ for all simulations compared to REF and changes in CO_2, air-sea CO_2 exchange and DIC inventory (Table 4), which are only slightly less than those found for the PE ratios. As for other carbon export efficiency estimates, LFN and LFA show only minor changes compared to REF, while in K&E (BAL) the difference of C-DISEQ to the one obtained for REF is negative (positive), accompanied by higher (lower) surface ocean pCO_2, negative (positive) air-sea CO_2 fluxes, and lower (higher) oceanic DIC inventories.

5. Long-Term Trends

[39] One drawback of the current study is that a 100 year simulation is too short to reach a new equilibrium. The deep ocean adjusts rather on a millennial timescale, consequently, particle fluxes may still undergo minor rearrangements in response. However, for all simulations, except for BAL, the annual mean air-sea CO_2 flux is already close to equilibrium after 100 years. One might assume that on the timescale of ocean mixing a progressive accumulation (depletion) of DIC in deep waters should result in higher (lower) surface ocean pCO_2 and thus stronger outgassing (uptake) of CO_2. A model study by *Schneider et al.* [2004] has run a comparable experiment into equilibrium, demonstrating that under a more efficient downward POC transport and in the absence of changes in alkalinity or circulation, the vertical DIC gradient in the water column is increased, resulting in a permanently higher oceanic DIC inventory.

[40] To address the question to what extent the results of the present study have to be attributed to the transient state after only 100 years of integration the simulation BAL was

Table 5. Long-Term Trends of pCO_2, CO_2-Flux, DIC Inventory, and Particle Flux Efficiency Indices for BAL

Experiment	pCO_2 (ppm)	CO_2-Flux (GtC/a)	DIC Inventory (GtC)	TEBUE	TEFRA	PE_{100}	$PIC:POC_{100}$	NO_3-GRAD	$CDISEQ_{100}$ (GtC)
REF	272.8	−0.33	35765	0.40	0.02	0.26	0.03	0.57	11.04
BAL(100 years)	269.4	0.83	35915	0.59	0.15	0.62	0.01	0.67	11.21
BAL (900 years)	277.8	−0.03	35994	0.79	0.26	0.59	0.01	0.45	7.05

extended until about 900 years, as this simulation was still most away from equilibrium in terms of air-sea CO_2-flux after 100 years. The results show that the trend of BAL toward more efficient POC flux and thus higher carbon transport toward depth is maintained even when surface pCO_2 and air-sea CO_2 exchange equilibrate (Figure 5 and Table 5). At the same time reduced surface NO_3 concentrations are accompagnied by a stabilization of PP around 10 GtC/a. The persistence of these reorganizations is also shown by the increased oceanic DIC inventory after 900 years (Table 5) and except for NO_3-GRAD and C-$DISEQ_{100}$ all efficiency measures still indicate more effective downward transport of organic carbon (Table 5). The later decrease of C-$DISEQ_{100}$ is consistent with equilibration of air-sea CO_2-exchange while the decrease of NO_3-GRAD toward the end can be explained by a slight increase PP below 100 m.

[41] A further point, which was also not taken into account by *Schneider et al.* [2004], is the fact that there is no feedback with the atmosphere from the air-sea CO_2 exchange. For example in BAL the ocean has accumulated more than 150 GtC already after 100 years of model integration. This should cause a reduction of the atmospheric pCO_2 on the order of 70 ppm, which in turn would reduce the surface ocean ΔpCO_2 and thereby oceanic CO_2 uptake. On the other hand, upwelling and outgassing of progressively DIC enriched deep waters would act into the opposite direction. The assumption of an unlimited source/sink reservoir of CO_2 in the atmosphere provides a further unrealistic (external) forcing, however, as there is neither sensitivity of the climate system nor of biological productivity to CO_2, this is acceptable for a sensitivity study.

6. Conclusions

[42] The present study has illustrated that changes in the vertical transport of particulate organic and inorganic carbon in the ocean leave their imprint on surface ocean properties like nutrients, productivity, pCO_2, air-sea CO_2 exchange and the global DIC inventory. Without assessing the reliability of each particle flux parameterization applied [see *Gehlen et al.*, 2006], the results clearly show that next to POC flux it is just as important to regard variations in PIC flux, as the net effect of particle flux reorganizations on surface ocean pCO_2 is rather a combination of changes in DIC and alkalinity.

[43] The application of a large number of different estimates for the efficiency of vertical carbon transport has demonstrated, that the choice of efficiency measure is dependent on the purpose of its application. If the task is to estimate biological turnover efficiency, a dimensionless one-parameter (POC) estimate like TE may be appropriate. With regard to air-sea CO_2 exchange, however, several parameters need to be taken into account to capture the changes invoked by both DIC and alkalinity. A good example are the reasonably high correlation coefficients obtained for PIC:POC ratios. Surprisingly, the PE ratio, which is also dimensionless, but at least includes two different quantities (productivity and export) yields highest correlation coefficients with surface ocean CO_2 parameters among the efficiency estimates tested in this study.

[44] In summary, changes in the vertical transport of particulate organic and inorganic carbon in the water column strongly interact with surface ocean pCO_2 and thus directly affect air-sea CO_2 exchange and oceanic carbon storage. Next to POC fluxes, changes in the transport of PIC need to be taken into account, because of two reasons: ballasting material and surface water chemistry (calcium carbonate counter pump). This is of particular importance against the background of a probable reduction of marine pelagic calcification due to ocean acidification [*Gehlen et al.*, 2007; *Orr et al.*, 2005]. To be able to estimate particle flux changes from observations more large-scale long-term observations are necessary.

[45] **Acknowledgments.** This work was supported by EU grants EVK2-CT-2001-00100 (EU-FP5 RTD project ORFOIS) and GOCE-511176 (FP6 RTP project CARBOOCEAN) by the European Commission. This is publication 2953 from LSCE.

References

Armstrong, R. A., C. Lee, J. I. Hedges, S. Honjo, and S. G. Wakeham (2002), A new mechanistic model for organic carbon fluxes in the ocean based on the quantitative association of POC with ballast minerals, *Deep Sea Res., Part II*, *49*, 219–236.

Aumont, O., and L. Bopp (2006), Globalizing results from ocean in situ iron fertilization studies, *Global Biogeochem. Cycles*, *20*, GB2017, doi:10.1029/2005GB002591.

Behrenfeld, M. J., et al. (2006), Climate-driven trends in contemporary ocean productivity, *Nature*, *444*, 752–755.

Bopp, L., P. Monfray, O. Aumont, J. L. Dufresne, H. Le Treut, G. Madec, L. Terray, and J. C. Orr (2001), Potential impact of climate change on marine export production, *Global Biogeochem. Cycles*, *15*, 81–99.

Boyd, P. W., and S. C. Doney (2002), Modelling regional responses by marine pelagic ecosystems to global climate change, *Geophys. Res. Lett.*, *29*(16), 1806, doi:10.1029/2001GL014130.

Boyd, P. W., and T. W. Trull (2007), Understanding the export of biogenic particles in oceanic waters: Is there consensus?, *Progr. Oceanogr.*, *72*, 276–312, doi:10.1016/j.pocean.2006.10.007.

Buesseler, K. O., et al. (2007), Revisiting carbon flux through the ocean's twilight zone, *Science*, *316*, 456–570.

Carr, M.-E., et al. (2006), A comparison of global estimates of marine primary production from ocean color, *Deep Sea Res.*, *53*, 741–770.

Conkright, M. E., R. A. Locarnini, H. E. Garcia, T. D. O'Brien, T. P. Boyer, C. Stephens, and J. I. Antonov (2002), *World Ocean Atlas 2001: Objective Analyses, Data Statistics, and Figures*, CD-ROM documentation, NOAA, Silver Spring, Md.

Dunne, J. P., R. A. Armstrong, A. Gnanadesikan, and J. L. Sarmiento (2005), Empirical and mechanistic models for the particle export ratio, *Global Biogeochem. Cycles*, *19*, GB4026, doi:10.1029/2004GB002390.

Francois, R., S. Honjo, R. Krishfield, and S. Manganini (2002), Factors controlling the flux of organic carbon to the bathypelagic zone of the ocean, *Global Biogeochem. Cycles*, *16*(4), 1087, doi:10.1029/2001GB001722.

Gehlen, M., L. Bopp, N. Emprin, O. Aumont, C. Heinze, and O. Ragueneau (2006), Reconciling surface ocean productivity, export fluxes and sediment composition in a global biogeochemical ocean model, *Biogeosciences*, *3*, 521–537.

Gehlen, M., R. Gangstø, B. Schneider, L. Bopp, O. Aumont, and C. Ethe (2007), The fate of pelagic $CaCO_3$ production in a high CO_2 ocean: A model study, *Biogeosciences*, *4*, 505–519.

Gust, G., A. F. Michaels, A. Johnson, W. G. Deuser, and W. Bowles (1994), Mooring line motions and sediment trap hydrodynamics: In situ intercomparison of three common deployment designs, *Deep Sea Res.*, *41*, 831–857.

Howard, M. T., A. M. E. Winguth, C. Klaas, and E. Maier-Reimer (2006), Sensitivity of ocean carbon tracer distributions to particulate organic flux paraterizations, *Global Biogeochem. Cycles*, *20*, GB3011, doi:10.1029/2005GB002499.

Kähler, P., and E. Bauerfeind (2001), Organic particles in a shallow sediment trap: Substantial loss to the dissolved phase, *Limnol. Oceanogr.*, *46*(3), 719–723.

Klaas, C., and D. E. Archer (2002), Association of sinking organic matter with various types of mineral ballast in the deep sea: Implications for the rain ratio, *Global Biogeochem. Cycles*, *16*(4), 1116, doi:10.1029/2001GB001765.

Kriest, I., and G. T. Evans (2000), A vertically resolved model for phytoplankton aggregation, *Proc. Indian Acad. Sci. Earth Planet. Sci.*, *109*, 453–469.

Kriest, I., and A. Oschlies (2008), On the treatment of particulate organic matter sinking in large-scale models of marine biogeochemical cycles, *Biogeosciences*, *5*, 55–72.

Laws, E. A., P. G. Falkowski, W. O. Smith, and H. Ducklow (2000), Temperature effects on export production in the open ocean, *Global Biogeochem. Cycles*, *14*(4), 1231–1246.

Le Quéré, C., et al. (2007), Saturation of the Southern Ocean CO_2 sink due to recent climate change, *Science*, *316*, 1735–1738.

Madec, G., P. Delecluse, M. Imbard, and M. Lévy (1998), OPA 8.1 ocean general circulation model reference manual, *Notes du Pôle de Modélisation*, *11*, technical report, IPSL, Paris.

Mikaloff Fletcher, S. E., et al. (2007), Inverse estimates of the oceanic sources and sinks of natural CO_2 and the implied oceanic carbon transport, *Global Biogeochem. Cycles*, *21*, GB1010, doi:10.1029/2006GB002751.

Najjar, R. G., et al. (2007), Impact of circulation on export production, dissolved organic matter and dissolved oxygen in the ocean: Results from OCMIP-2, *Global Biogeochem. Cycles*, *21*, GB3007, doi:10.1029/2006GB002857.

Orr, J. C., et al. (2005), Anthropogenic ocean acidification over the twenty-first century and its impact on calcifying organisms, *Nature*, *437*, 681–686, doi:10.1038/nature04095.

Oschlies, A., and P. Kähler (2004), Biotic contribution to air-sea fluxes of CO_2 and O_2 and its relation to new production, export production, and net community production, *Global Biogeochem. Cycles*, *18*, GB1015, doi:10.1029/2003GB002094.

Passow, U., and C. De La Rocha (2006), Accumulation of mineral ballast on organic aggregates, *Global Biogeochem. Cycles*, *20*, GB1013, doi:10.1029/2005GB002579.

Sarmiento, J. L., and N. Gruber (2006), *Ocean Biogeochemical Dynamics*, Princeton Univ. Press, Princeton, N. J.

Sarmiento, J. L., et al. (2004), Response of ocean ecosystems to climate warming, *Global Biogeochem. Cycles*, *18*, GB3003, doi:10.1029/2003GB002134.

Schlitzer, R. (2000), Applying the adjoint method for global biogeochemical modeling, in *Inverse Methods in Biogeochemical Cycles*, edited by P. Kasibhatla et al., pp. 107–124, AGU, Washington, D. C.

Schneider, B., R. Schlitzer, G. Fischer, and E.-M. Nöthig (2003), Depth-dependent elemental compositions of particulate organic matter (POM) in the ocean, *Global Biogeochem. Cycles*, *17*(2), 1032, doi:10.1029/2002GB001871.

Schneider, B., A. Engel, and R. Schlitzer (2004), Effects of depth- and CO_2-dependent C:N ratios of particulate organic matter (POM) on the marine carbon cycle, *Global Biogeochem. Cycles*, *18*, GB2015, doi:10.1029/2003GB002184.

Solomon, S., et al. (2007), Technical summary, in *Climate Change 2007: The Physical Science Basis. Contribution of Working Group I to the Fourth Assessment Report of the Intergovernmental Panel on Climate Change*, edited by S. Solomon et al., pp. 1–996, Cambridge Univ. Press, Cambridge, UK.

Takahashi, T., et al. (2002), Global sea-air CO_2 flux based on climatological surface ocean pCO_2, and seasonal biological and temperature effects, *Deep Sea Res.*, *2*(49), 1601–1622.

Usbeck, R., R. Schlitzer, G. Fischer, and G. Wefer (2003), Particle fluxes in the ocean: Comparison of sediment trap data with results from inverse modeling, *J. Mar. Syst.*, *39*, 167–183.

Volk, T., and M. I. Hoffert (1985), Ocean carbon pumps: Analysis of relative strengths and efficiencies in ocean-driven atmospheric CO_2 changes, in *The Carbon Cycle and Atmospheric CO_2: Natural Variations Archean to Present*, edited by E. Sundquist and W. S. Broecker, *Geophys. Monogr. Ser.*, vol. 32, pp. 99–110, AGU, Washington D. C.

Wanninkhof, R. (1992), Relationship between wind speed and gasexchange over the ocean, *J. Geophys. Res.*, *97*, 7373–7382.

L. Bopp and M. Gehlen, Laboratoire du Climat et de l'Environnement (LSCE), L'Orme des Merisiers Bât. 712, F-91191 Gif sur Yvette, France.

B. Schneider, Institute of Geosciences, University of Kiel, Ludewig-Meyn-Strasse 10, D-24098 Kiel, Germany. (bschneider@gpi.uni-kiel.de)